Hindawi
International Journal of Aerospace Engineering
Volume 2019, Article ID 4749109, 10 pages
https://doi.org/10.1155/2019/4749109

Research Article

Autopilot Design for a Compound Control Small-Scale Solid Rocket in the Initial Stage of Launch

Tian Dong, Changjian Zhao, and Zhiguo Song

China Academy of Launch Vehicle Technology, Beijing 100076, China

Correspondence should be addressed to Tian Dong; 326264694@qq.com

Received 12 November 2018; Accepted 20 January 2019; Published 6 March 2019

Academic Editor: Teng Wu

In this paper, an autopilot design method for a compound control small-scale solid rocket is proposed. The rocket has multiple actuators, including a flexible nozzle for pitching and yawing channels, aerodynamic fins for rolling channel, and lateral thrusters which work in on-off mode for all three channels. In order to keep the aircraft steady in the initial stage of launch when the dynamic pressure is low, the autopilot is aimed at optimizing the cooperation among the actuators. Firstly, without considering the discontinuous lateral thrust, the control law for flexible nozzle and aerodynamic fins is achieved via the sliding mode control approach. On this basis, an object to be controlled with choiceness is obtained for the lateral thrusters controlled loop. Secondly, the operation logic of lateral thrusters is programmed, regarding rolling moment as priority. Thirdly, after a continuous controller is obtained, a discretization method for the lateral thrusters control law is designed combining the characteristics of sliding mode control and Lyapunov's stableness theorem. Finally, the fundamental cause why compound control improves the system stability is given theoretically. Simulation results validate the improved response performance and robustness against uncertainties and disturbance of the autopilot.

1. Introduction

Traditional aircraft controlled only by aerodynamic fins is hard to keep steady in the initial stage of launch, because the aerodynamic fin control efficiency is low for low-velocity aircraft, which leads to a difficulty in aircraft design [1]. Therefore, some aircrafts apply the flexible nozzles into pitching and yawing channels to make the control magnitude independent of velocity. However, the flexible nozzle cannot provide a control moment for the rolling channel. The instability of the rolling channel would lead to bad performance of the autopilot, because of aerodynamic couplings [2]. Therefore, it is necessary to provide sufficient control for the advanced aircrafts to keep steady for three channels.

Another effective method to promote the performance of the control system is to employ both traditional aerodynamic fins and lateral thrusters at the same time. Recently, a lot of research on high-altitude interception has been done to improve the autopilot's performance by this method [3]. The advantage of this compound control technology is to provide sufficient control through lateral thrust, especially when the dynamic pressure gets low, and make full use of the nonworking medium consuming air force. It will be meaningful to apply this compound control technology in the initial stage of launch to keep stability against disturbance. However, the lateral thrusters are usually used in the pitching and yawing channels instead of the rolling channel.

In order to make full use of the aerodynamic fins, the flexible nozzles, and the lateral thrusters and avoid their disadvantages, in this paper, the flexible nozzle is used in the pitching and yawing channels, the aerodynamic fins are applied into the rolling channel, and the lateral thrusters are employed in all the three channels.

A well-designed compound-control autopilot shall take advantage of all actuators. The main difficulty during design is that the aerodynamic fins and the flexible nozzle provide continuous control force while the lateral thrusters work in on-off mode, which makes the whole control system to be a discrete/continuous hybrid system. The design methods for the hybrid control system have been studied in many researches. In the early stage, Hirokawa et al. [4] decompose the MIMO control system into a feedback and feedforward

controller design problem. The feedback controller is designed using the algebraic approach, and the feedforward controller is designed to achieve the minimum fuel consumption independently. The control allocation method is used to optimize the cooperation in many researches. Xu et al. [5] take advantage of the robust adaptive sliding sector to produce a virtual control effort signal and use a control allocator based on the L2 optimal control allocation strategy to distribute the virtual signal to the two pairs of actuators. Mathavaraj et al. [6] allocate the control command in the daisy chain mode, which chooses to use the aerodynamic fin system as much as possible in order to save fuel for the lateral thruster system. Bi et al. [7] provide an ADRC-based controller which obtains the required control moment according to the angle of attack tracking deviation then allocate the respective commands to the aerodynamic deflection and lateral thruster using the dynamic control allocation. Li and Zhou [8] propose a θ-D feedback controller to steer the aircraft to track reference acceleration commands based on the linear-like structure, which ensures the asymptotic stability based on Lyapunov's theorem. Zhao et al. [9] complete the aerodynamic fin controlled loop based on the concept of finite time stability, then using a backstepping approach to design a lateral thruster control law. Generally, most researches focus on the control method and specific allocation of the two actuators, while few of them study the stability issue caused by discrete characteristics of lateral thrust.

To promote the compound control performance for small-scale solid rockets, in this paper, the control method is proposed creatively. At first, a continuous controller is designed by the sliding mode control approach without considering the discrete characteristic of the lateral thrusters. Then, a operation logic of the lateral thrusters is optimized that provides a control moment for the rolling channel as a priority. Finally, according to the operation logic, the lateral thrust control law is discretized under the premise of the stable system based on Lyapunov's theorem. Simulation results validate the effectiveness of the proposed approach and the improved performance compared to the traditional autopilot without lateral thrusters.

2. Dynamic Model of the Compound Controlled Rocket

Consider that the aircraft has a flexible nozzle which controls the yaw and pitch motions and aerodynamic fins which control the roll motion. Also, eight lateral thrusters are arranged in a lap with a 90-degree interval. Four of them provide lateral thrust parallel to the z axis of the body coordinate system, and the other four provide lateral thrust parallel to y axis of the body coordinate, as Figure 1 illustrates. x, y, z represent the axes of the body coordinate system to describe the force and moment provided by lateral thrusters.

The thrusters can provide control force for the yawing and pitching channels and work in pairs to generate a rolling moment for the rolling channel. Without loss of generality, suppose each thruster is able to generate a thrust $\bar{P}$, with the arm of x_{2e} relative to the x axis. The specific number, force, and moment of each thruster are shown in Table 1. For example, if the lateral thruster No. 1 is working, it will produce a moment of $\bar{P} \cdot x_{2e}$ parallel to the x axis, "0" force relative to the y axis, and force $\bar{P}$ relative to the z axis.

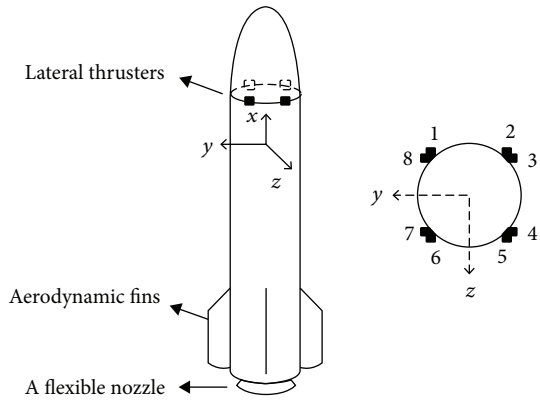

Figure 1: The diagram of the layout of lateral thrusters.

Table 1: Specific information of each thruster.

Thruster	No. 1	No. 2	No. 3	No. 4	No. 5	No. 6	No. 7	No. 8
x (moment)	$\bar{P}x_{2e}$	$-\bar{P}x_{2e}$	$\bar{P}x_{2e}$	$-\bar{P}x_{2e}$	$\bar{P}x_{2e}$	$-\bar{P}x_{2e}$	$\bar{P}x_{2e}$	$-\bar{P}x_{2e}$
y (force/N)	0	0	$\bar{P}$	$\bar{P}$	0	0	$-\bar{P}$	$-\bar{P}$
z (fore/N)	$\bar{P}$	$\bar{P}$	0	0	$-\bar{P}$	$-\bar{P}$	0	0

Based on the sphere Earth model, the six-degree-of-freedom dynamic equations are established as follows, neglecting the rotation of the Earth.

$$\begin{bmatrix} \dot{x} \\ \dot{y} \\ \dot{z} \end{bmatrix} = \begin{bmatrix} V_x \\ V_y \\ V_z \end{bmatrix},$$

$$\begin{bmatrix} \frac{dV_x}{dt} \\ \frac{dV_y}{dt} \\ \frac{dV_z}{dt} \end{bmatrix} = \frac{\mathbf{G_B}}{m} \left\{ \begin{bmatrix} P_e \\ P_e\delta_\varphi \\ -P_e\delta_\psi \end{bmatrix} + \begin{bmatrix} \frac{\partial C_A}{\partial \delta_\gamma} qS_m \\ \frac{\partial C_N}{\partial \delta_\gamma} qS_m \\ \frac{\partial C_Z}{\partial \delta_\gamma} qS_m \end{bmatrix} \delta_\gamma + \begin{bmatrix} 0 \\ +2\dot{m}\omega_{z1}x_{1e} \\ -2\dot{m}\omega_{y1}x_{1e} \end{bmatrix} \right\} + \begin{bmatrix} g_x \\ g_y \\ g_z \end{bmatrix}, \quad (1)$$

with

$$\mathbf{G_B} = \begin{bmatrix} \cos\varphi\cos\psi & \cos\varphi\sin\psi\sin\gamma - \sin\varphi\cos\gamma & \cos\varphi\sin\psi\cos\gamma + \sin\varphi\sin\gamma \\ \sin\varphi\cos\psi & \cos\varphi\cos\gamma + \sin\varphi\sin\psi\sin\gamma & \sin\varphi\sin\psi\cos\gamma - \cos\varphi\sin\gamma \\ -\sin\psi & \cos\psi\sin\gamma & \cos\psi\cos\gamma \end{bmatrix},$$

$$\begin{bmatrix} \dot{\gamma} \\ \dot{\psi} \\ \dot{\varphi} \end{bmatrix} = \begin{bmatrix} \omega_{x1} + \dot{\varphi}\sin\psi \\ \omega_{y1}\cos\gamma - \omega_{z1}\sin\gamma \\ \dfrac{\omega_{y1}\sin\gamma + \omega_{z1}\cos\gamma}{\cos\psi} \end{bmatrix}, \tag{2}$$

$$\begin{bmatrix} I_x & 0 & 0 \\ 0 & I_y & 0 \\ 0 & 0 & I_z \end{bmatrix} \begin{bmatrix} \dfrac{d\omega_{x1}}{dt} \\ \dfrac{d\omega_{y1}}{dt} \\ \dfrac{d\omega_{z1}}{dt} \end{bmatrix} + \begin{bmatrix} (I_z - I_y)\omega_{z1}\omega_{y1} \\ (I_x - I_z)\omega_{x1}\omega_{z1} \\ (I_y - I_x)\omega_{y1}\omega_{x1} \end{bmatrix} = \left\{ \begin{bmatrix} \dfrac{\partial C_{mx}}{\partial\delta_\gamma} qS_m l_k \\ \dfrac{\partial C_{my}}{\partial\delta_\gamma} qS_m l_k \\ \dfrac{\partial C_{mz}}{\partial\delta_\gamma} qS_m l_k \end{bmatrix} + \begin{bmatrix} -\dfrac{(\partial C_{lp}/\partial\delta_\gamma) qS_m l_k^2 \omega_{x1}}{V} \\ -\dfrac{(\partial C_{nr}/\partial\delta_\gamma) qS_m l_k^2 \omega_{y1}}{V} \\ -\dfrac{(\partial C_{mq}/\partial\delta_\gamma) qS_m l_k^2 \omega_{z1}}{V} \end{bmatrix} \right\} \delta_\gamma \tag{3}$$

$$+ \begin{bmatrix} 0 \\ -P_e x_{1e}\delta_\psi \\ -P_e x_{1e}\delta_\varphi \end{bmatrix} + \begin{bmatrix} p_g x_{2e} \\ p_z x_{3e} \\ -p_y x_{3e} \end{bmatrix} - \begin{bmatrix} \dot{I}_x\omega_{x1} \\ \dot{I}_y\omega_{y1} \\ \dot{I}_z\omega_{z1} \end{bmatrix} + \dot{m} \begin{bmatrix} 0 \\ -x_{1e}^2\omega_{y1} \\ -x_{1e}^2\omega_{z1} \end{bmatrix},$$

where x, y, z are the position components in the launch coordinate system, V_x, V_y, V_z are the velocity components in the launch coordinate system, m is the current mess of the aircraft, P_e is the thrust of the main engine, $\delta_\varphi, \delta_\psi, \delta_\gamma$ are the flexible nozzle deflection angles for pitching and yawing channels and aileron deflection angle, C_A, C_N, C_Z are the coefficients of aerodynamic force of the aircraft, q means the dynamic pressure, S_m is the reference area of the aircraft, $\omega_{x1}, \omega_{y1}, \omega_{z1}$ are angular velocity components observed in the body coordinate system, x_{1e} is the distance from the engine nozzle to the center of mess, g_x, g_y, g_z are the gravitational coefficients in three axes, φ, ψ, γ are the three attitude angles, I_x, I_y, I_z are the components of the rotational inertia, C_{mx}, C_{my}, C_{mz} are the coefficients of the aircraft's aerodynamic moment, l_k is the reference aerodynamic length of the aircraft, C_{lp}, C_{nr}, C_{mq} are the coefficients of the aerodynamic damping, p_g is the equivalent lateral thrust in the rolling channel, with an arm of x_{2e} relative to the rolling axis, and p_y and p_z are the equivalent lateral thrusts in the pitching channel and the yawing channel, respectively, with an arm of x_{3e} relative to the pitching axis or yawing axis.

3. Compound Control System Design

The sliding mode method is a nonlinear control method which has great robustness against the model parameter variation and disturbance [10, 11]. It is applicable to the condition of large aerodynamic disturbance caused by the lateral thrusters. Accordingly, the aerodynamic surface controlled loop is designed at first via the sliding mode control approach. Suppose the lateral thrust is zero, the sliding mode surface is designed as

$$\mathbf{s} = \begin{bmatrix} c_1(\varphi_c - \varphi) + \dot{\varphi}_c - \dot{\varphi} \\ c_2(\psi_c - \psi) + \dot{\psi}_c - \dot{\psi} \\ c_3(\gamma_c - \gamma) + \dot{\gamma}_c - \dot{\gamma} \end{bmatrix} = \begin{bmatrix} s_1 \\ s_2 \\ s_3 \end{bmatrix}, \tag{4}$$

where elements in c are the controlling parameters that are greater than zero, and $\varphi_c, \psi_c, \gamma_c$ denote the control command of attitude angles. In order to improve the

dynamic performance, the exponential reaching law has been chosen as

$$\dot{\mathbf{s}} = \begin{bmatrix} c_1(\dot{\varphi}_c - \dot{\varphi}) + \ddot{\varphi}_c - \ddot{\varphi} \\ c_2(\dot{\psi}_c - \dot{\psi}) + \ddot{\psi}_c - \ddot{\psi} \\ c_3(\dot{\gamma}_c - \dot{\gamma}) + \ddot{\gamma}_c - \ddot{\gamma} \end{bmatrix} = \begin{bmatrix} -\varepsilon_1 \operatorname{sgn} s_1 - k_1 s_1 \\ -\varepsilon_2 \operatorname{sgn} s_2 - k_2 s_2 \\ -\varepsilon_3 \operatorname{sgn} s_3 - k_3 s_3 \end{bmatrix}, \quad (5)$$

where ε, k are the control parameters with elements greater than zero. Substituting Equation (2) and Equation (3) into Equation (5) successively, the flexible nozzle deflection for the pitching channel, the flexible nozzle deflection for the yawing channel, and the aileron deflection angle $\delta_\phi, \delta_\psi, \delta_\gamma$ are solved.

$$\begin{bmatrix} \delta_\varphi \\ \delta_\psi \\ \delta_\gamma \end{bmatrix} = \begin{bmatrix} \frac{\cos\gamma}{I_z \cos\psi} P_e x_{1e} & 0 & -\frac{A_\varphi \cdot \cos\gamma}{I_z \cos\psi} \\ 0 & \frac{\cos\gamma}{I_y} P_e x_{1e} & -\frac{A_\psi \cdot \cos\gamma}{I_y} \\ 0 & 0 & -\frac{A_\gamma}{I_x} \end{bmatrix}^{-1} \cdot \left\{ \begin{bmatrix} -\varepsilon_1 \operatorname{sgn} s_1 - k_1 s_1 \\ -\varepsilon_2 \operatorname{sgn} s_2 - k_2 s_2 \\ -\varepsilon_3 \operatorname{sgn} s_3 - k_3 s_3 \end{bmatrix} + \begin{bmatrix} -c_1\left(\dot{\varphi}_c - \frac{\omega_z \cos\gamma}{\cos\psi}\right) - \ddot{\varphi}_c + \frac{\omega_x \omega_y \cos\gamma}{\cos\psi} - \frac{\cos\gamma}{\cos\psi}\frac{1}{I_z}\left[(I_y - I_x)\omega_y\omega_x + I_z\omega_z + \dot{m}x_e^2\omega_z\right] \\ -c_2(\dot{\psi}_c - \omega_y\cos\gamma) - \ddot{\psi}_c + \omega_x\omega_z\cos\gamma - \frac{\cos\gamma}{I_y}\left[(I_x - I_z)\omega_x\omega_z + I_y\omega_y + \dot{m}x_e^2\omega_y\right] \\ -c_3(\dot{\gamma}_c - \omega_x) - \ddot{\gamma}_c - \frac{1}{I_x}\left[(I_z - I_y)\omega_z\omega_y + I_x\omega_x\right] \end{bmatrix} \right\}, \quad (6)$$

with

$$\begin{bmatrix} A_\gamma \\ A_\psi \\ A_\varphi \end{bmatrix} = \left\{ \begin{bmatrix} \frac{\partial C_{mx1}}{\partial \delta_\gamma} q S_m l_k \\ \frac{\partial C_{my1}}{\partial \delta_\gamma} q S_m l_k \\ \frac{\partial C_{mz1}}{\partial \delta_\gamma} q S_m l_k \end{bmatrix} + \begin{bmatrix} -\frac{(\partial C_{lp}/\partial\delta_\gamma) q S_m l_k^2 \omega_{x1}}{V} \\ -\frac{(\partial C_{nr}/\partial\delta_\gamma) q S_m l_k^2 \omega_{y1}}{V} \\ -\frac{(\partial C_{mq}/\partial\delta_\gamma) q S_m l_k^2 \omega_{z1}}{V} \end{bmatrix} \right\}. \quad (7)$$

On this basis, the inner loop is considered as an object to be controlled with choiceness in the lateral thruster controlled loop. A continuous controller is designed via the sliding mode control approach firstly, without the consideration of the discontinuous feature of the lateral thrust. Similar to the aerodynamic surface control loop, the sliding mode surface is designed as

$$\mathbf{s}' = \begin{bmatrix} c_1'(\varphi_c - \varphi) + \dot{\varphi}_c - \dot{\varphi} \\ c_2'(\psi_c - \psi) + \dot{\psi}_c - \dot{\psi} \\ c_3'(\gamma_c - \gamma) + \dot{\gamma}_c - \dot{\gamma} \end{bmatrix} = \begin{bmatrix} s_1' \\ s_2' \\ s_3' \end{bmatrix}, \quad (8)$$

where c' are controlling parameters with elements greater than zero. Then, the derivative of $\mathbf{s}'$ is

$$\dot{\mathbf{s}}' = \begin{bmatrix} c_1'(\dot{\varphi}_c - \dot{\varphi}) + \ddot{\varphi}_c - \ddot{\varphi} \\ c_2'(\dot{\psi}_c - \dot{\psi}) + \ddot{\psi}_c - \ddot{\psi} \\ c_3'(\dot{\gamma}_c - \dot{\gamma}) + \ddot{\gamma}_c - \ddot{\gamma} \end{bmatrix}. \quad (9)$$

In order to improve the dynamic performance, the exponential reaching law has been chosen as

$$\dot{\mathbf{s}}' = \begin{bmatrix} -\varepsilon_1' \operatorname{sgn} s_1' - k_1' s_1' \\ -\varepsilon_2' \operatorname{sgn} s_2' - k_2' s_2' \\ -\varepsilon_3' \operatorname{sgn} s_3' - k_3' s_3' \end{bmatrix}, \quad (10)$$

where ε', k' are the controlling parameters with elements greater than zero. Substituting Equation (2), Equation (3), and Equation (10) into Equation (9) successively, the continuous lateral thrust p_y, p_z, p_g are

$$\begin{bmatrix} p_y \\ p_z \\ p_g \end{bmatrix} = \begin{bmatrix} \left\{ -\varepsilon_1' \operatorname{sgn} s_1' - k_1' s_1' - \begin{bmatrix} c_1'\left(\dot{\varphi}_c - \dfrac{\omega_z \cos\gamma}{\cos\psi}\right) + \ddot{\varphi}_c - \dfrac{\omega_x \omega_y \cos\gamma}{\cos\psi} - \\ \dfrac{\cos\gamma}{I_z \cos\psi}\begin{bmatrix} (I_x - I_y)\omega_x\omega_y + C\delta_\gamma - \\ P_e x_{3e}\delta_\varphi - \dot{I}_z\omega_z - \dot{m}x^2_{1e}\omega_z \end{bmatrix} \end{bmatrix} \right\} \dfrac{I_z \cos\psi}{x_{3e}\cos\gamma} \\ \left\{ -\varepsilon_2' \operatorname{sgn} s_2' - k_2' s_2' - \begin{bmatrix} c_2'(\dot{\psi}_c - \omega_y \cos\gamma) + \ddot{\psi}_c - \omega_x\omega_z \cos\gamma - \\ \dfrac{\cos\gamma}{I_y}\begin{bmatrix} (I_z - I_x)\omega_x\omega_z + B\delta_\gamma - \\ P_e x_{3e}\delta_\psi - \dot{I}_y\omega_y - \dot{m}x^2_{1e}\omega_y \end{bmatrix} \end{bmatrix} \right\} \dfrac{-I_y}{x_{3e}\cos\gamma} \\ \left\{ -\varepsilon_3' \operatorname{sgn} s_3' - k_3' s_3' - \begin{Bmatrix} c_3'(\dot{\gamma}_c - \omega_x) + \ddot{\gamma}_c - \\ \dfrac{1}{I_x}\begin{bmatrix} -(I_z - I_y)\omega_z\omega_y + A\delta_\gamma \\ -\dot{I}_x\omega_x \end{bmatrix} \end{Bmatrix} \right\} \dfrac{-I_x}{x_{2e}} \end{bmatrix}, \tag{11}$$

where $\delta_\varphi, \delta_\psi, \delta_\gamma$ are obtained by Equation (6).

Finally, considering the lateral thruster work in on-off mode, the operation logic of lateral thrusters is designed to satisfy the rolling channel demand preferentially, because the flexible nozzle would provide relatively more control in the pitching and yawing channels, and the main purpose for the lateral thrusters is to provide sufficient control for the rolling channel. The additional effect of the operation logic design for lateral thrusters is to decrease the deflection of the flexible nozzle, which can save energy for the main engine. According to the considerations above and the layout of lateral thrusters, one possible control combination for the three channels is shown in Table 2.

According to the operation logic of the lateral thrusters, the continuous p_y, p_z, p_g are discretized according to the following rules which can guarantee the stability proved by Lyapunov's stableness theorem.

In order to describe the discretization method, denote the desired lateral thrust obtained by Equation (11) as

$$\mathbf{u_d} = \begin{bmatrix} p_y & p_z & p_g \end{bmatrix}^T. \tag{12}$$

Considering the limitation of the discrete operation logic, the lateral thrusters are hard to provide the desired control input precisely. The actual lateral thrusts $\mathbf{u}$ are described as

$$\mathbf{u} = \mathbf{u_d} - \mathbf{d_c}, \tag{13}$$

where $\mathbf{d_c} = [d_{cy}, d_{cz}, d_{cx}]^T$ denotes the thrust adjustment during the discretization. It is obvious that the most desired lateral thrust is between two practical values, neglecting the input saturation. The relationship among $\mathbf{u_d}$ and those two practical thrust values $\mathbf{u_l}$ and $\mathbf{u_u}$ is

$$u_{l_i} < u_{d_i} < u_{u_i}, \quad i = 1, 2, 3. \tag{14}$$

For example, if $\bar{P} = 50N$ and the desired lateral thrust for the rolling channel is 150 N, the practical values $u_{l_3} = 100N$ and $u_{u_3} = 200N$, according to the operation logic.

Therefore, the thrust adjustment has two possible values, which are defined as

$$\begin{aligned} d_{cl_i} &= u_{d_i} - u_{l_i} > 0, \quad i = 1, 2, 3, \\ d_{cu_i} &= u_{d_i} - u_{u_i} < 0. \end{aligned} \tag{15}$$

Take advantage of Lyapunov's stableness theorem, to determine the actual thrust adjustments $\mathbf{d_c}$. Consider a Lyapunov function candidate as

$$V = \frac{1}{2}\mathbf{s}'^T\mathbf{s}'. \tag{16}$$

So the derivative of V is

$$\dot{V} = \mathbf{s}'^T\dot{\mathbf{s}}'. \tag{17}$$

It is obvious that if $\mathbf{s}'T\dot{\mathbf{s}}' < 0$, the system is asymptotically stable. Substituting Equation (2), Equation (3), Equation (6), and Equation (11) into Equation (9) successively, one can obtain that

$$\dot{\mathbf{s}}' = \begin{bmatrix} -\varepsilon_1' \operatorname{sgn} s_1' - k_1' s_1' - b_y d_{cy} \\ -\varepsilon_2' \operatorname{sgn} s_2' - k_2' s_2' + b_z d_{cz} \\ -\varepsilon_3' \operatorname{sgn} s_3' - k_3' s_3' + b_x d_{cx} \end{bmatrix}, \tag{18}$$

Table 2: The possible control combination of lateral thrusters.

Modes	Mode 1	Mode 2	Mode 3	Mode 4	Mode 5	Mode 6	Mode 7	Mode 8	Mode 9
P_g/N	0	0	0	0	$(\pm)2\bar{P}$	$(\pm)2\bar{P}$	$(\pm)2\bar{P}$	$(\pm)2\bar{P}$	$(\pm)4\bar{P}$
P_y/N	$(\pm)2\bar{P}$	0	$(\pm)2\bar{P}$	$(\pm)\bar{P}$	0	$(\pm)2\bar{P}$	0	$(\pm)\bar{P}$	0
P_z/N	0	$(\pm)2\bar{P}$	$(\pm)2\bar{P}$	$(\pm)\bar{P}$	0	0	$(\pm)2\bar{P}$	$(\pm)\bar{P}$	0

with

$$\begin{bmatrix} b_y \\ b_z \\ b_x \end{bmatrix} = \begin{bmatrix} \dfrac{\cos\gamma}{I_z \cos\psi} x_{3e} \\ \dfrac{\cos\gamma}{I_y} x_{3e} \\ \dfrac{1}{I_x} x_{3e} \end{bmatrix}. \tag{19}$$

b_y, b_z, b_x are greater than zero, according to the physical truth. When $\dot{s}_i' < 0$ for $i = 1, 2, 3$, to make sure that $\mathbf{s}'^T \dot{\mathbf{s}}' < 0$, let $s_i' > 0$ for $i = 1, 2, 3$. Therefore, the thrust adjustment $\mathbf{d_c}$ is solved as

$$\mathbf{d_c} = \begin{bmatrix} d_{cy} = \begin{cases} d_{cl}, \text{if } \operatorname{sgn}\left(s_1'\right) = 1 \\ d_{cu}, \text{if } \operatorname{sgn}\left(s_1'\right) = -1 \end{cases} \\ d_{cz} = \begin{cases} d_{cu}, \text{if } \operatorname{sgn}\left(s_2'\right) = 1 \\ d_{cl}, \text{if } \operatorname{sgn}\left(s_2'\right) = -1 \end{cases} \\ d_{cx} = \begin{cases} d_{cu}, \text{if } \operatorname{sgn}\left(s_3'\right) = 1 \\ d_{cl}, \text{if } \operatorname{sgn}\left(s_3'\right) = -1 \end{cases} \end{bmatrix}. \tag{20}$$

Substituting Equation (20) into Equation (13), the actual control inputs of lateral thrusters are obtained.

Similar to the sliding-mode control, the discretization method makes the lateral thrusters turn on and off frequently when $\mathbf{s}'$ is close to $\mathbf{0}$, which wastes a lot of fuel and may cause the undesired vibration. The decreasing chattering approach for sliding-mode control can also be used when the thrust adjustment is determined.

4. Stability Analysis

The aircraft is a MIMO nonlinear system with input saturation. Define the control input saturation as

$$\operatorname{sat}(u_i) = \begin{cases} u_{\max}, & u_i \geq u_{\max}, \quad i = 1, 2, 3, \\ u_i, & u_{\min} < u_i < u_{\max}, \\ u_{\min}, & u_i \leq u_{\min}, \end{cases} \tag{21}$$

where $\operatorname{sat}(\mathbf{u})$ is the actual control input, and $u_{\max} > 0$ and $u_{\min} < 0$ are saturation amplitudes. The part beyond saturation $\boldsymbol{\Delta}$ can be described as

$$\boldsymbol{\Delta} = \mathbf{u} - \operatorname{sat}(\mathbf{u}). \tag{22}$$

Consider $\boldsymbol{\Delta}$ as perturbations of the system. Substituting $[\delta_\varphi\ \delta_\psi\ \delta_\gamma]$ and $[p_y\ p_z\ p_g]$ obtained from Equation (6) and Equation (11) into Equation (21), the practical control input $\operatorname{sat}(\mathbf{u_\delta})$ and $\operatorname{sat}(\mathbf{u_p})$ are got. Then substituting $\operatorname{sat}(\mathbf{u_\delta})$ and $\operatorname{sat}(\mathbf{u_p})$ into Equation (9), one can obtain

$$\dot{\mathbf{s}}' = \begin{bmatrix} -\varepsilon_1' \operatorname{sgn} s_1' - k_1' s_1' \\ -\varepsilon_2' \operatorname{sgn} s_2' - k_2' s_2' \\ -\varepsilon_3' \operatorname{sgn} s_3' - k_3' s_3' \end{bmatrix} + \mathbf{B_\delta}\boldsymbol{\Delta_\delta} + \mathbf{B_p}\boldsymbol{\Delta_p}, \tag{23}$$

where

$$\mathbf{B_\delta} = \begin{bmatrix} \dfrac{\cos\gamma}{I_z \cos\psi} P_e x_{1e} & 0 & -\dfrac{A_\varphi \cdot \cos\gamma}{I_z \cos\psi} \\ 0 & \dfrac{\cos\gamma}{I_y} P_e x_{1e} & -\dfrac{A_\psi \cdot \cos\gamma}{I_y} \\ 0 & 0 & -\dfrac{A_\gamma}{I_x} \end{bmatrix},$$

$$\mathbf{B_p} = \begin{bmatrix} \dfrac{\cos\gamma}{I_z \cos\psi} x_{3e} & 0 & 0 \\ 0 & -\dfrac{\cos\gamma}{I_y} x_{3e} & 0 \\ 0 & 0 & -\dfrac{x_{2e}}{I_x} \end{bmatrix}. \tag{24}$$

Consider a Lyapunov function candidate as

$$V = \frac{1}{2} \mathbf{s}'^T \mathbf{s}'. \tag{25}$$

The derivative of V is

$$\dot{V} = \mathbf{s}'^{T}\dot{\mathbf{s}}' = \sum_{i=1}^{3}\left(-\varepsilon_i'|s_i'| - k_i's_i'^2\right) + \left(\mathbf{B}_{\boldsymbol{\delta}}\boldsymbol{\Delta}_{\boldsymbol{\delta}} + \mathbf{B}_{\mathbf{p}}\boldsymbol{\Delta}_{\mathbf{p}}\right)^T\mathbf{s}' \leq \sum_{i=1}^{3}\left(-\varepsilon_i'|s_i'| - k_i's_i'^2\right) + \sum_{i=1}^{3}\left(\left|\left(\mathbf{B}_{\boldsymbol{\delta}}\boldsymbol{\Delta}_{\boldsymbol{\delta}} + \mathbf{B}_{\mathbf{p}}\boldsymbol{\Delta}_{\mathbf{p}}\right)_i\right| \cdot |s_i'|\right). \tag{26}$$

During the realistic mission, $|(\mathbf{B}_{\boldsymbol{\delta}}\boldsymbol{\Delta}_{\boldsymbol{\delta}} + \mathbf{B}_{\mathbf{p}}\boldsymbol{\Delta}_{\mathbf{p}})_i| \cdot |s_i'|$ is unknown but actually bounded. Thus, there exists a positive constant D that satisfies $\sum_{i=1}^{3}(|(\mathbf{B}_{\boldsymbol{\delta}}\boldsymbol{\Delta}_{\boldsymbol{\delta}} + \mathbf{B}_{\mathbf{p}}\boldsymbol{\Delta}_{\mathbf{p}})_i| \cdot |s_i'|) < D$. And Equation (26) can be rewritten as

$$\dot{V} \leq \sum_{i=1}^{3}\left(-\varepsilon_i'|s_i'| - k_i's_i'^2\right) + D. \tag{27}$$

Further,

$$\dot{V} \leq -\sum_{i=1}^{3}k_i's_i'^2 + D \leq -\sum_{i=1}^{3}k_{\min}' \cdot s_i'^2 + D = -2k_{\min}'V + D, \tag{28}$$

with

$$k_{\min}' = \min\begin{pmatrix} k_1' & k_2' & k_3' \end{pmatrix}. \tag{29}$$

According to Equation (28),

$$\dot{V} \leq -2k_{\min}'\left(V - \frac{D}{2k_{\min}'}\right). \tag{30}$$

Since $k_{\min}'$ and D are both constants,

$$\frac{d\left(V - \left(D/2k_{\min}'\right)\right)}{dt} \leq -2k_{\min}'\left(V - \frac{D}{2k_{\min}'}\right). \tag{31}$$

When $V > D/2k_{\min}'$, let $\lambda \triangleq \ln\left(V - (D/2k_{\min}')\right)$, then

$$\dot{\lambda} \leq -2k_{\min}', \tag{32}$$

so

$$\lambda \leq \lambda_0 - 2k_{\min}'t. \tag{33}$$

Substituting $\lambda = \ln\left(V - (D/2k_{\min}')\right)$ into Equation (33),

$$\ln\left(V - \frac{D}{2k_{\min}'}\right) \leq \ln\left(V_0 - \frac{D}{2k_{\min}'}\right) - 2k_{\min}'t. \tag{34}$$

Then,

$$V - \frac{D}{2k_{\min}'} \leq \left(V_0 - \frac{D}{2k_{\min}'}\right)e^{-2k_{\min}'t}, \tag{35}$$

so

$$V \leq e^{-2k_{\min}'t}V_0 + \frac{D}{2k_{\min}'}\left(1 - e^{-2k_{\min}'t}\right). \tag{36}$$

As is known to all, $0 < e^{-2k_{\min}'t} \leq 1$,

$$V \leq V_0 + \frac{D}{2k_{\min}'}. \tag{37}$$

When $V < D/2k_{\min}'$, let $\lambda \triangleq \ln\left(-V + (D/2k_{\min}')\right)$; according to Equation (31),

$$\dot{\lambda} \geq -2k_{\min}', \tag{38}$$

so

$$\lambda \geq \lambda_0 - 2k_{\min}'t. \tag{39}$$

Substituting $\lambda = \ln\left(-V + (D/2k_{\min}')\right)$ into Equation (39),

$$\ln\left(-V + \frac{D}{2k_{\min}'}\right) \geq \ln\left(-V_0 + \frac{D}{2k_{\min}'}\right) - 2k_{\min}'t, \tag{40}$$

so

$$V \leq e^{-2k_{\min}'t}V_0 + \frac{D}{2k_{\min}'}\left(1 - e^{-2k_{\min}'t}\right), \tag{41}$$

which also leads to Equation (37).

When $V = D/2k_{\min}'$, Equation (37) is correct, as well.

Therefore, the system is uniformly ultimately bounded. All the signals in the closed-loop systems converge to a compact set Ω which is defined as

$$\boldsymbol{\Omega} = \left\{s_1', s_2', s_3', \varphi, \psi, \gamma, \dot{\varphi}, \dot{\psi}, \dot{\gamma} \mid V \leq V_0 + \frac{D}{2k_{\min}'}\right\}. \tag{42}$$

According to Equation (27), if D is not too great, there exists ε' and k' with positive elements that guarantee $\dot{V} < 0$, and the system will be asymptotically stable. The compound control improves the total capacity of the autopilot, which increases the saturation amplitudes and therefore decreases the perturbation. This is the reason why this compound control autopilot insures the stability while improving the dynamic performance for the aircraft.

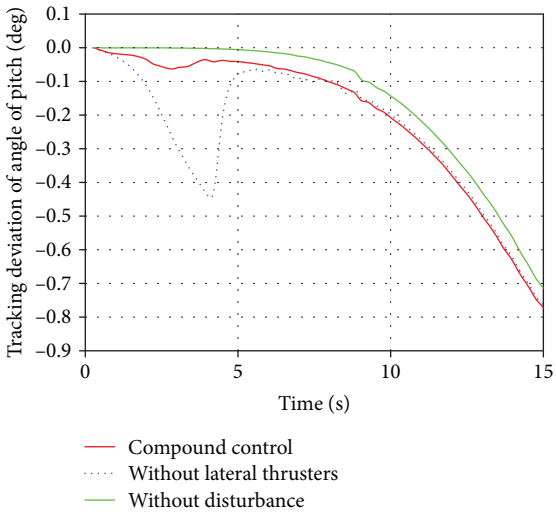

Figure 2: Tracking deviation of angle of pitch in the initial stage of launch.

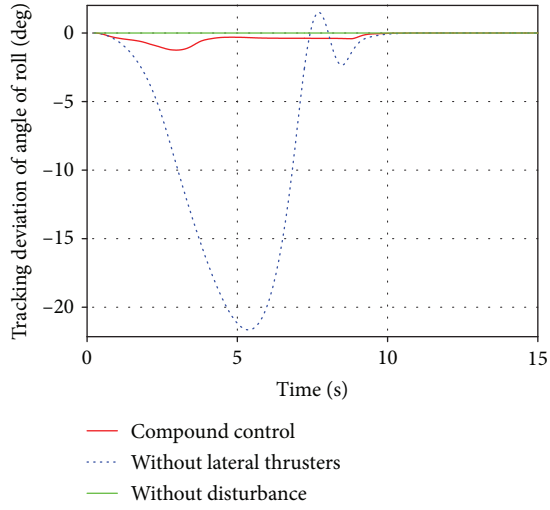

Figure 4: Tracking deviation of angle of roll in the initial stage of launch.

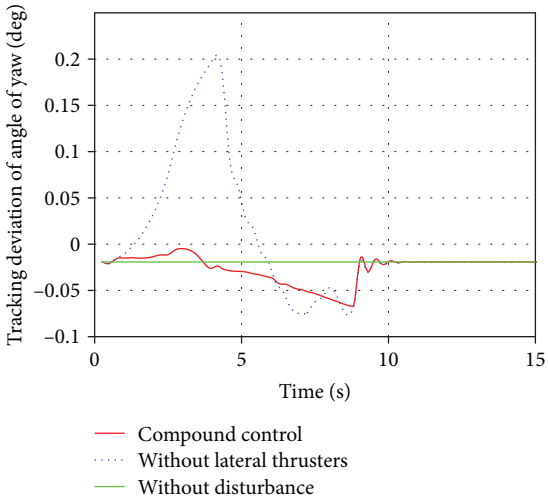

Figure 3: Tracking deviation of angle of yaw in the initial stage of launch.

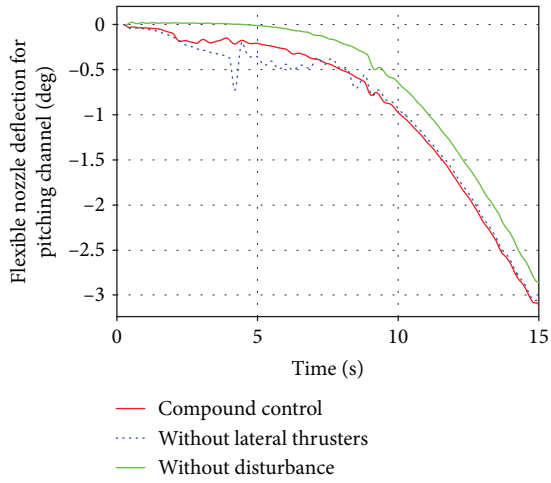

Figure 5: Variation of nozzle deflection for pitching channel in the initial stage of launch.

5. Simulations and Analysis

Numerical results are obtained by using a six-degree-of-freedom aircraft model which is launched from the ground with the 90° angle of pitch. The aircraft tracks a predefined schema trajectory given by a period of attitude control commands ϕ_c, ψ_c, γ_c, where ψ_c, γ_c keep zero, and φ_c decreases from 90° to shape the trajectory. Steady wind and wind shear are considered in the simulation to evaluate the performance of the compound controller.

The numerical results of the initial stage of launch are shown in Figures 2–10. The red lines represent the results of compound control. The blue lines show the results of the flexible nozzle and aerodynamic surface control, without lateral thrusters. The green lines describe the nominal condition where there is no disturbance.

As can be seen from Figures 2–4, the wind disturbance increases the tracking deviation, but the compound controller can still hold the system steady. The tracking deviation of the angle of pitch does not converge to zero, which is necessary, because the control demand is varying to shape the trajectory. The wind disturbance influences more at the beginning of the launch when the velocity is low. So the deflection angles of the nozzle and the aileron get great and the lateral thrusters keep working, as is presented from Figures 5–10.

Furthermore, the comparison between compound control and control without lateral thrusters shows that the tracking deviations and actuator deflection under compound control are both smaller. In each channel, the actuators cooperate to generate a control moment in the same direction. And the direction of control moment is defined by Equation (3).

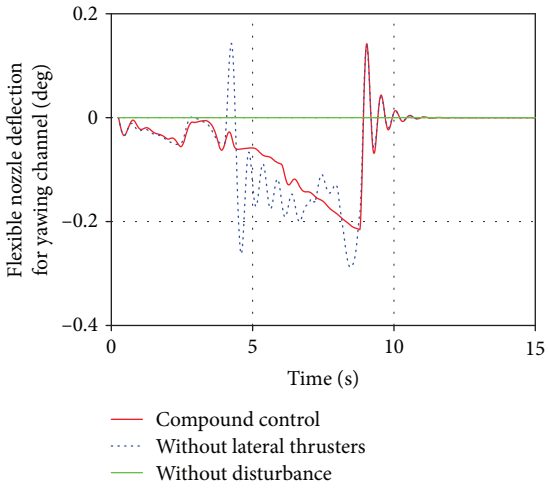

Figure 6: Variation of nozzle deflection for yawing channel in the initial stage of launch.

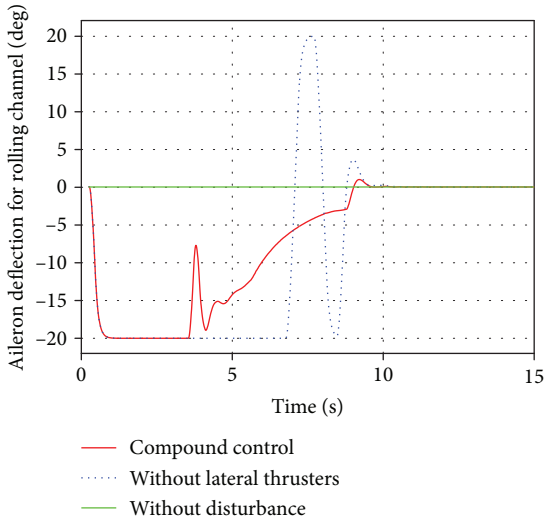

Figure 7: Variation of aileron deflection in the initial stage of launch.

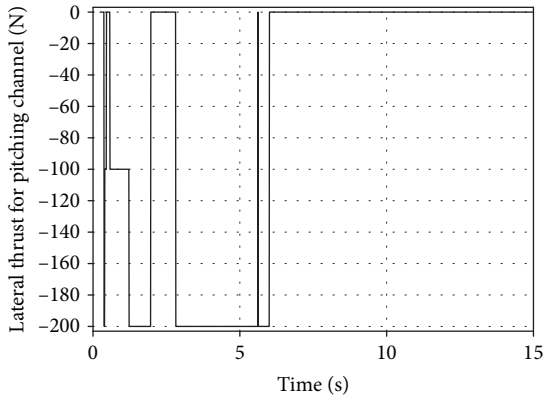

Figure 8: Variation of lateral thrust P_y in the initial stage of launch.

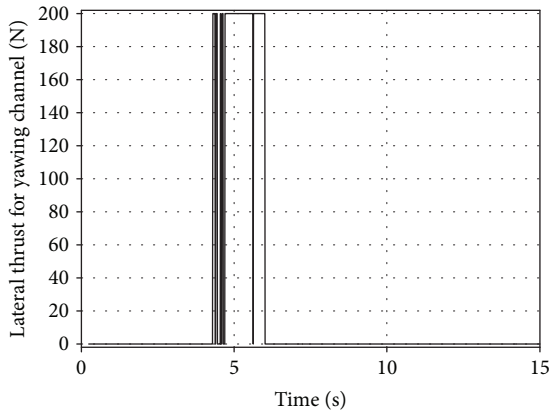

Figure 9: Variation of lateral thrust P_z in the initial stage of launch.

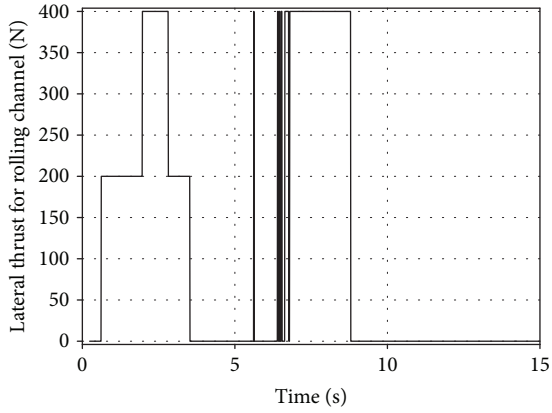

Figure 10: Variation of lateral thrust P_g in the initial stage of launch.

Specifically, In Figure 2, the tracking deviation of the angle of pitch under compound control is smaller than that under control without lateral thrusters, because of the control moment provided by lateral thrusters in Figure 8 and the decreased couplings when the angle of roll is near zero in Figure 4. As is shown in Figure 5, the deflection of the flexible nozzle under compound control is smaller than that under control without lateral thrusters which saves energy for the main engine. The flexible nozzle deflection for the pitching channel is negative which provides positive control moment. The corresponding lateral thrust for the pitching channel is negative which generates a positive control moment. It demonstrates that under the compound control law, the flexible nozzle and lateral thrusters cooperated with each other and there is no undesirable counteracting. The same conclusion can be seen in the simulation results of the yawing channel in Figures 3, 6, and 9. The tracking deviation of the angle of roll and the usage of actuators for the rolling channel are shown in Figures 4, 7, and 10. The tracking deviation of the angle of roll is apparently smaller, and aileron saturation time decreases under compound control. This is because the control efficiency of ailerons is low when the velocity is low in the initial stage of launch, and the control moment provided by lateral thrusters is of the same direction as that induced by

ailerons. This increases the actuators' saturation amplitudes and therefore decreases the tracking deviation.

It is demonstrated that the compound controller improves the performance of the autopilot by realizing the cooperation among actuators. That validates this compound control method is which effective to use the flexible nozzle, aerodynamic fins, and lateral thrusters to achieve a better response against disturbance and improve the stability of the aircraft.

6. Conclusions

This paper proposes a control scheme for aircrafts in the initial stage of launch. An autopilot design method is described for an aircraft with a flexible nozzle, aerodynamic fins, and lateral thrusters. This method is based on a nonlinear model, and the stability is guaranteed in each step of the design process. Simulation shows that the actuators are cooperated to improve the control which enhances the stability of the aircraft. Further, the disturbance from the lateral thrusters and other realistic impacts should be taken into consideration to improve the accuracy of modelling.

Data Availability

The data used to support the findings of this study are available from the corresponding author upon request.

Conflicts of Interest

The authors declare that there is no conflict of interest regarding the publication of this paper.

References

[1] L. K. Abbas, D. Chen, and X. Rui, "Numerical calculation of effect of elastic deformation on aerodynamic characteristics of a rocket," *International Journal of Aerospace Engineering*, vol. 2014, Article ID 478534, 11 pages, 2014.

[2] M. Rezazadeh Mohammadi, M. Fathi Jegarkandi, and A. Moarrefianpour, "Robust roll autopilot design to reduce couplings of a tactical missile," *Aerospace Science and Technology*, vol. 51, pp. 142–150, 2016.

[3] D. Ridgely, D. Drake, L. Triplett, and C. Geise, "Dynamic control allocation of a missile with tails and reaction jets," in *AIAA Guidance, Navigation and Control Conference and Exhibit*, pp. 1–32, Hilton Head, SC, USA, August 2007.

[4] R. Hirokawa, K. Sato, and S. Manabe, "Autopilot design for a missile with reaction-jet using coefficient diagram method," in *AIAA Guidance, Navigation, and Control Conference and Exhibit*, pp. 1–8, Montreal, Canada, August 2001.

[5] B. Xu, D. Zhou, Z. Liang, and G. Zhou, "Robust adaptive sliding sector control and control allocation of a missile with aerodynamic control surfaces and reaction jets," *Proceedings of the Institution of Mechanical Engineers, Part G: Journal of Aerospace Engineering*, vol. 231, no. 3, pp. 397–406, 2016.

[6] S. Mathavaraj, O. Halbe, and R. Padhi, "Robust control of a reusable launch vehicle in reentry phase using model following neuro-adaptive design," in *AIAA Guidance, Navigation, and Control Conference*, pp. 1–25, Toronto, ON, Canada, August 2010.

[7] Y. T. Bi, F. H. He, and Y. Yao, "Design of blended lateral thrust and aerodynamic surface control strategy for agile missile," *Journal of Jilin University (Engineering and Technology Edition)*, vol. 41, no. 2, pp. 590–596, 2011.

[8] Q. Li and D. Zhou, "Nonlinear autopilot design for interceptors with tail fins and pulse thrusters via θ-D approach," *Journal of Systems Engineering and Electronics*, vol. 25, no. 2, pp. 273–280, 2014.

[9] M. Y. Zhao, M. Y. Wei, and Q. R. He, "Research on method of lateral jet and aerodynamic fins compound control based on finite time stability and backstepping approach," *Journal of Astronautics*, vol. 31, no. 9, pp. 2157–2164, 2010.

[10] M. Bahrami, B. Ebrahimi, and G. R. Ansarifar, "Sliding mode observer and control design with adaptive parameter estimation for a supersonic flight vehicle," *International Journal of Aerospace Engineering*, vol. 2010, Article ID 474537, 9 pages, 2010.

[11] N. Ramos-Pedroza, W. MacKunis, and M. Reyhanoglu, "A sliding mode LCO regulation strategy for dual-parallel Underactuated UAV systems using synthetic jet actuators," *International Journal of Aerospace Engineering*, vol. 2015, Article ID 795348, 7 pages, 2015.